JGR Planets

RESEARCH ARTICLE
10.1029/2021JE006954

Local Time Dependence of Jupiter's Polar Auroral Emissions Observed by Juno UVS

Thomas Greathouse[1], Randy Gladstone[1,2], Maarten Versteeg[1], Vincent Hue[1], Joshua Kammer[1], Rohini Giles[1], Michael Davis[1], Scott Bolton[1], Steven Levin[3], John Connerney[4], Jean-Claude Gérard[5], Denis Grodent[5], Bertrand Bonfond[5], Emma Bunce[6], and Marissa F. Vogt[7]

[1]Southwest Research Institute, San Antonio, TX, USA, [2]University of Texas at San Antonio, San Antonio, TX, USA, [3]Jet Propulsion Laboratory, Pasadena, CA, USA, [4]NASA Goddard Space Flight Center, Greenbelt, MD, USA, [5]Université de Liège, LPAP - STAR Institute, Liège, Belgium, [6]University Leicester, Leicester, UK, [7]Center for Space Physics, Boston University, Boston, MA, USA

Key Points:

- Jupiter's bright and variable polar auroral swirl region emissions are observed to be weak/absent from 22 to 7 hr local solar time
- Higher color ratios observed within the polar swirl region relative to the dark/active regions suggest differing physical mechanisms
- Emissions from the newly defined polar collar (dark/active regions) correlate with magnetic local time regardless of local solar time

Supporting Information:

Supporting Information may be found in the online version of this article.

Correspondence to:

T. Greathouse,
tgreathouse@swri.edu

Citation:

Greathouse, T., Gladstone, R., Versteeg, M., Hue, V., Kammer, J., Giles, R., et al. (2021). Local time dependence of Jupiter's polar auroral emissions observed by Juno UVS. *Journal of Geophysical Research: Planets*, *126*, e2021JE006954. https://doi.org/10.1029/2021JE006954

Received 13 MAY 2021
Accepted 27 OCT 2021

Author Contributions:

Conceptualization: Thomas Greathouse, Emma Bunce
Data curation: Thomas Greathouse, Randy Gladstone, Maarten Versteeg, Vincent Hue, Joshua Kammer, Michael Davis
Formal analysis: Thomas Greathouse, Jean-Claude Gérard, Denis Grodent, Bertrand Bonfond, Marissa F. Vogt
Funding acquisition: Randy Gladstone, Scott Bolton, Steven Levin, John Connerney
Investigation: Thomas Greathouse, Randy Gladstone, Scott Bolton, Steven Levin, John Connerney
Methodology: Thomas Greathouse, Randy Gladstone, Jean-Claude Gérard, Denis Grodent, Bertrand Bonfond, Emma Bunce

Abstract Auroral brightness and color ratio imagery, captured using the Juno mission's Ultraviolet Spectrograph, display intense emissions poleward of Jupiter's northern main emission, and these are split into two distinctly different spectral or "color ratio" regimes. The most poleward region, designated the "swirl region" by Grodent et al. (2003), https://doi.org/10.1029/2003ja010017, exhibits a high color ratio, while low color ratio emissions are found within the collar around the swirl region but still poleward of the main emission. We confirm the apparent strong magnetospheric local time control within the polar collar (Grodent et al., 2003, https://doi.org/10.1029/2003ja010017), with the dusk side bright "active region" emissions extending from ~11 to 22 hr of magnetospheric local time. These bright emissions dim by at least an order of magnitude between ~0 and 11 hr magnetospheric local time, in the midnight to dawn side "dark region." This magnetospheric local time structure holds true even when the entire northern oval is located on the night side of the planet (in ionospheric local time), a geometry unstudied prior to Juno, as it is unobservable from Earth. The swirl region brightens at ionospheric dawn (~5–7 ionospheric local time) and diminishes or completely disappears at ionospheric local times of ~20–22 hr. Finally, the southern auroral polar emissions appear to share all of the local time dependencies of its northern counterpart, but at a reduced intensity.

Plain Language Summary The Juno mission is in a polar orbit around Jupiter, which allows imaging of the planet's polar auroras at a wide range of local times. In this study, we use data from Juno's Ultraviolet Spectrograph (UVS) to study how different regions of the auroras vary with the solar geometry. We find that there are two auroral regions with distinct local time behavior: the "polar collar," which is located just inside the main auroral oval, and the "swirl region," which is located within the polar collar. As expected, the brightness of the polar collar varies with the magnetospheric local time, which is the local time relative to the magnetic pole and is a measure of the position of events occurring within the magnetosphere. This is true regardless of solar illumination, when the northern oval is completely in sunlight or completely in the dark. In contrast, the swirl region brightness is instead correlated with the ionospheric local time, which is a measure of how sunlit the upper atmosphere is. The difference in local time control of these two regions, in addition to their distinct spectral signatures, suggests they are produced by significantly different processes in the middle to outer magnetosphere.

1. Introduction

Jupiter's ultraviolet aurorae provide a visual display of some of the complex interplay of Jupiter's strong magnetic field with the plasmas within the Jovian system. The Juno mission, with its highly elliptical polar orbit, was designed, in part, to bring a powerful package of in-situ and remote sensing instruments low over Jupiter's polar regions to probe the details of the high latitude magnetosphere (Bagenal et al., 2017; Bolton et al., 2017). The Juno Ultraviolet Spectrograph (UVS; Gladstone et al., 2017) is an imaging spectrograph covering 68–210 nm. The instrument is used to produce brightness and color ratio maps of Jupiter's ultraviolet auroral H_2 emissions, providing information about the total flux and the average energy of precipitating electrons (Yung et al., 1982), respectively. These maps can be directly compared to measurements made by Juno's in-situ instruments (Allegrini, Mauk, et al., 2020; Ebert et al., 2019; Gérard et al., 2019; Mauk et al., 2020; Szalay et al., 2020).

Resources: Joshua Kammer, Michael Davis
Software: Thomas Greathouse, Marissa F. Vogt
Validation: Maarten Versteeg, Bertrand Bonfond
Visualization: Vincent Hue
Writing – original draft: Thomas Greathouse, Bertrand Bonfond
Writing – review & editing: Vincent Hue, Rohini Giles, Michael Davis, Scott Bolton, Steven Levin, John Connerney, Jean-Claude Gérard, Denis Grodent, Bertrand Bonfond, Marissa F. Vogt

In addition to providing context imaging for the in-situ instruments, UVS also provides unique views of Jupiter's aurorae unobtainable from the Hubble Space Telescope (HST; Grodent et al., 2018) or from Earth orbit in general (XMM, Chandra, or Hisaki). Due to Juno's polar orbit, UVS obtains near nadir views of Jupiter's aurorae, unlike the high zenith angle observations available with HST. Observations from HST are also limited to the planet's dayside, while UVS is able to provide observations at all local times. This makes Juno UVS uniquely suited to study the local time dependence of Jupiter's auroral emissions.

In this study, we present Juno UVS brightness and color ratio maps covering the full 24 hr range of local times and displaying the complex morphologies and local time behavior of the polar-most auroral emissions, that is, those emissions occurring poleward of Jupiter's main auroral ovals. Bright emissions from within the auroral ovals is rather unique to Jupiter; in contrast, the polar caps of Earth and Saturn are mostly dark. It is thus not surprising that the polar-most regions of the Jovian aurorae are also the most poorly understood. While quite variable, the total emitted power of the polar regions in the UV range usually accounts for 1/3 of the total emitted power from the whole aurora, and the power in this region is generally correlated with that of the main emission (Grodent et al., 2018; Nichols, Clarke, Gerard, & Grodent, 2009). Three sub-regions of Jupiter's polar UV aurora have been identified from HST images (Grodent et al., 2003): (a) the dark region on the dawn and night flanks of the main emissions, mostly devoid of UV emissions (e.g., Swithenbank-Harris et al., 2019); (b) the active region, where arcs and filaments (Nichols et al., 2007, 2017; Nichols, Clarke, Gerard, Grodent, & Hansen, 2009; Grodent et al., 2018), very bright flares (Waite et al., 2001) and quasi-periodic flares (Bonfond et al., 2011, 2016) are found; and (c) the swirl region in the center, peppered with dynamic and chaotic emissions that are strongly absorbed by methane (Bonfond et al., 2017). These complicated polar auroral emissions are magnetically linked to processes in the mid-to outer-magnetosphere well beyond ~20–30 Jovian radii, R_J, the expected equatorial distance to which the main auroral emission maps in the magnetosphere (e.g., Cowley & Bunce, 2001; Hill, 2001). Moreover, the size and location of the swirl region is compatible with the area open to the solar wind deduced from flux-equivalence magnetic mapping models (Bonfond et al., 2017; Vogt et al., 2011, 2015). We leave discussions of the main emission (another name for the auroral ovals) and equatorward emissions for future studies, while the satellite footprint aurora have already been addressed in several studies (Allegrini, Gladstone, et al., 2020; Hue, Greathouse, et al., 2019; Szalay et al., 2018, 2020).

2. Juno UVS Observations

2.1. Juno UVS Mapping

UVS is mounted on the spinning, 2-rpm, Juno spacecraft, nominally looking radially outward with an entrance slit oriented parallel to the spin axis. In this configuration, the slit sweeps across the sky, capturing a 7.2° (slit length) by 360° swath every 30 s. UVS has a "dog bone" shaped slit, with two wide segments on either side of a narrower segment. During each spin, a point source is observed for 17 ms if it falls within the wide slit and for 2 ms if it falls within the narrow slit. Using the scan mirror located at the telescope's entrance aperture allows for the adjustment of the field of view fore or aft of the Juno spin plane by up to ±30°, in increments of 0.74°, resulting in a field of regard of 67.2° × 360°, slightly more than half the sky. We create images of Jupiter's auroral regions by adding together multiple spins of data taken with differing scan mirror positions. The exact number of spins needed to create a full image depends on the range of the spacecraft to Jupiter and the scan mirror pointing plan defined by the UVS team uniquely for each perijove (PJ), a close pass of Juno to Jupiter in its highly elliptical orbit. In general, it takes ~40 spins worth of data when observing from a range of 1.6 R_J (an altitude of 0.6 R_J). Given the 2-rpm spin rate of Juno, this equates to ~20 min to build composite images of the aurora. This type of data acquisition has several important repercussions for UVS imagery. The first is that even if UVS targets a given location within Jupiter's aurora, the absolute best temporal sampling achievable by UVS is 30 s, with each look corresponding to a 17 ms integration time. The second is that our composite images of the aurora include observations obtained at significantly different times. One side of the image may be observed 10–20 min before the other side of the image. An example of the production of such images is included in the Movie S1 as multiple-spin animated GIF showing the addition of one spin at a time to produce a final image.

Brightness images presented here and in the supplementary material are calculated by integrating the observed H_2 emissions between 155 and 162 nm and multiplying by 8.1 (Gérard et al., 2019) to scale them to all H_2 Werner and Lyman emissions (e.g., Figure 1). This process capitalizes on the transparency of Jupiter's atmosphere between 155 and 162 nm and then leverages models of H_2 emissions caused by electron impact to derive the total amount

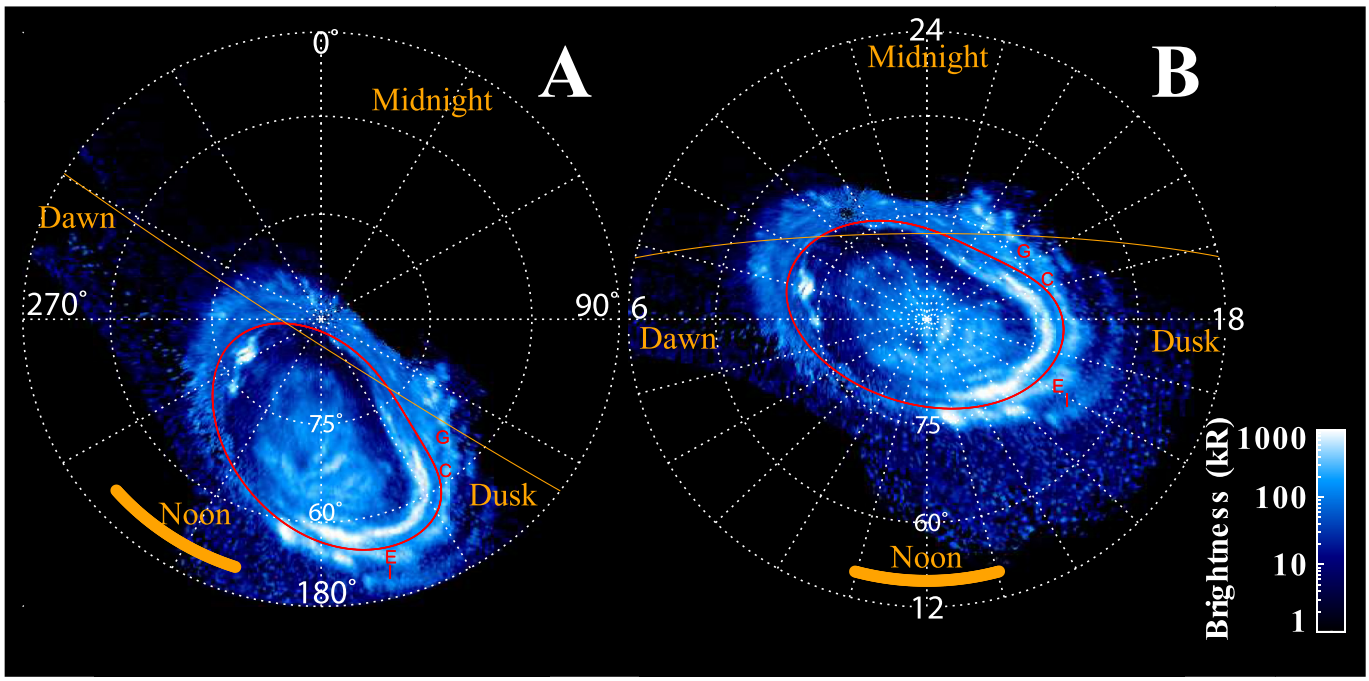

Figure 1. Panel A shows a brightness map of PJ5 data in System III coordinates. Panel B displays the same data in the magnetic dipole local time projection discussed in Section 2.2. The image was produced by integrating 101 spins of data, equivalent to an integration time period of 50.5 min. The local time map (B) is oriented such that noon at the midpoint of the integration time is directed down (toward the Sun), with dawn to the left and dusk to the right. The SIII longitudes in panel B have been replaced with magnetic local time values in hours. The terminator at 400 km altitude (orange thin line) is shown for the midpoint time while the thick orange line at the bottom shows the evolution of the Sun position over the integration time of the image (2 hr local time for Jupiter). The red ellipse in each panel demarcates the predicted Callisto footprint path, a representation of the mapping between the ionosphere and equatorial magnetosphere at ~26 R_J, using the JRM09 model.

of energy emitted from H_2 due to electron precipitation. Since the UVS instrument is a spectrograph, we simultaneously capture the UV emissions at all wavelengths between 68 and 210 nm (Hue, Gladstone, et al., 2019) with spectral resolution of ~1.3 nm within the narrow slit and 2–3 nm in the wide slits (T. K. Greathouse et al., 2013). This allows us to create accurate color ratio maps (e.g., Figure 2), where the color ratio is defined as the ratio of the radiance at 155–162 nm to the radiance at 125–130 nm (e.g., Bonfond et al., 2017). The wavelengths chosen for the color ratio are driven by methane's absorption spectrum, which has a long wavelength cutoff near 140 nm. The color ratio has long been used to infer the energy of the impacting electrons (e.g., Yung et al., 1982), with a higher color ratio implying higher energy electrons (Gustin et al., 2004). The link between the color ratio and the particle energy follows the reasonable expectation that higher energy particles will plunge further into Jupiter's atmosphere. At these greater depths, the H_2 emissions are absorbed by the overlying CH_4 in Jupiter's atmosphere, preferentially removing flux from the 125–130 nm region relative to that at 155–162 nm, causing an increase in the color ratio (e.g., Yung et al., 1982). The energy dependence inferred from the color ratio assumes that the vertical structure of Jupiter's atmosphere is uniform across the polar region. This assumption has recently come under scrutiny (Clark et al., 2018; Gérard et al., 2014; Sinclair et al., 2020).

2.2. Image Rotation From System III Coordinates to a Magnetospheric Local Time Projection

In this study, we are primarily interested in changes in auroral emission as a function of local time, something not easily explored from Earth. There are two local times that are of potential interest here: the ionospheric local time (solar local time derived for an auroral position as its System III longitude compared to the System III subsolar longitude) and the magnetospheric local time (the approximate local time of the point where a magnetic field line from a given auroral position crosses the jovigraphic equator). Since we expect the auroral emissions to be primarily controlled by magnetospheric local time, we make a change of coordinate system due to the offset of Jupiter's magnetic dipole relative to Jupiter's rotational axis, which is the axis of the System III coordinate system. In producing our images, we first integrate 101 spins (50.5 min = 2 hr of local time for Jupiter) of UVS observations into a cylindrical map projection using Jupiter's System III coordinate frame. The relatively long integrations

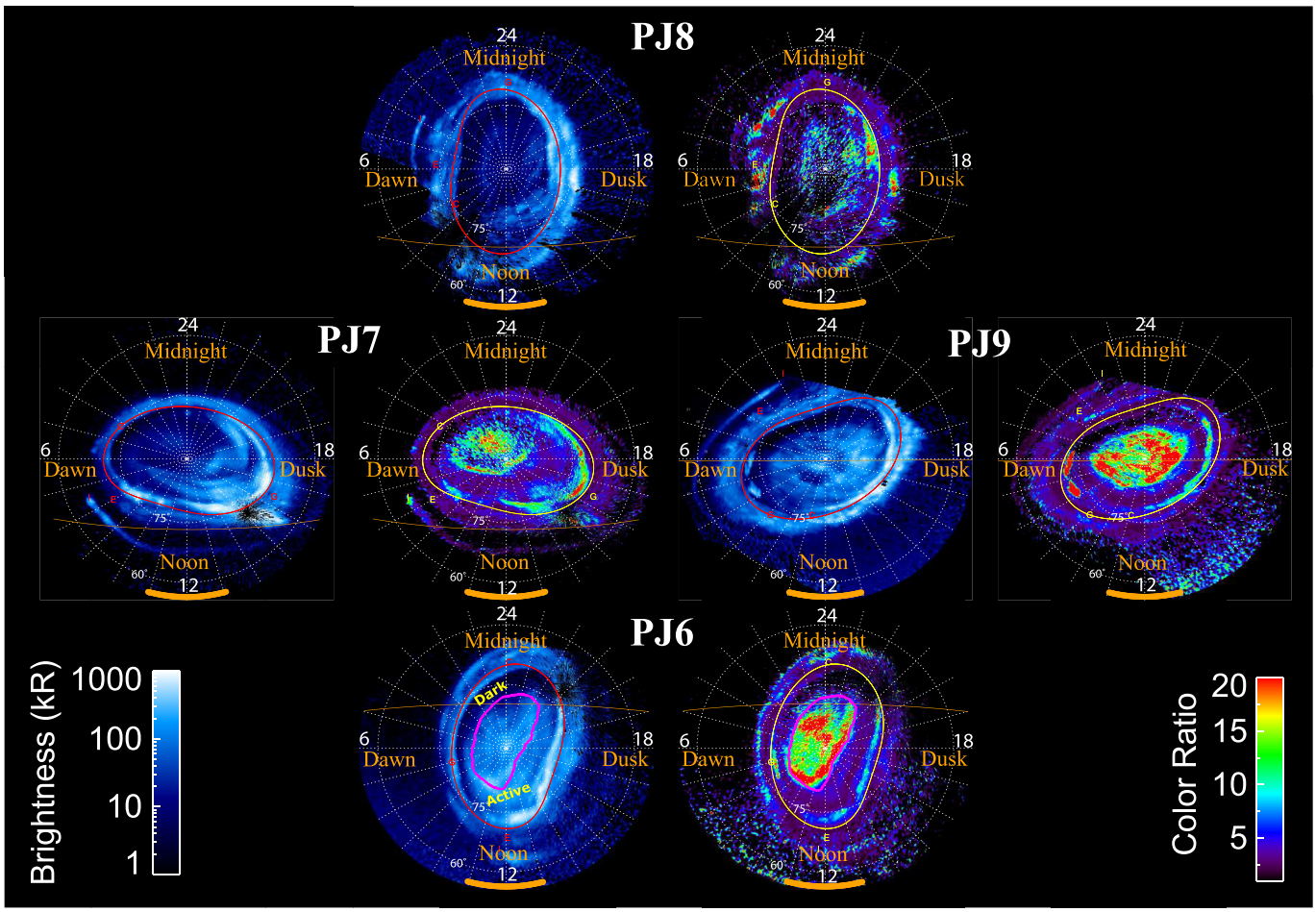

Figure 2. Maps of the northern auroral emissions with midnight, dawn, noon, and dusk (magnetic local time) labeled in orange, in both brightness on the left and color ratio on the right. Times and spacecraft/Jupiter geometric details for all figures are listed in Table 1. Terminator, Sun direction, integration time, etc. are all as described in Figure 1. The path of the Callisto footprint is shown by the red curve in the brightness plots and the yellow curve within the color ratio plots for clarity. The PJ pass number from which the data were collected are listed in the figure between the brightness and color ratio maps. The approximate demarcation between the swirl region and polar collar is outlined in magenta in the PJ6 data at the bottom of the figure, and the dark and active regions within the polar collar are labeled in the PJ6 brightness map.

were used to guarantee good areal coverage and high signal to noise for the images. However, a drawback is that any local time variations will be blurred by 1/12th of a Jovian rotation period. Following this, we perform a rotation to replace the System III coordinate axis by the centroid of the 30 R_J mapping of the JRM09 model of Connerney et al. (2018) for the north and south pole independently. The location of the northern centroid is 71.2° latitude and 178.1° longitude System III, while the southern centroid is −82.5° latitude and 30.4° longitude. These positions require Z- and *Y*-axis rotations for the northern auroral maps of −178.1° and 18.8°, respectively, about the IAU_Jupiter coordinate frame (Acton, 1996). The corresponding rotations for the southern map are −30.4° and −7.5°, respectively. We then project the maps into orthographic projections orienting them such that they appear fixed in magnetospheric local time to aid the eye in looking for the expected magnetospheric local time effects. Figure 1 shows the result of this change in coordinate frame for an image of Jupiter's northern aurora. Figure 1a shows a System III orthographic projection, and Figure 1b shows the same data after recentering on the northern 30 R_J centroid and rotating such that the subsolar longitude is toward the bottom of the page. This remapping leads to the main auroral oval approximately centered in the image. If we observe brightness variations organized in magnetospheric local time poleward of the main emission in this new coordinate frame, then these variations are likely controlled by what is happening at similar local times in the middle to outer magnetosphere.

Although the coordinates in Figure 1b relate to the magnetospheric local time, the image still contains information about the ionospheric local time. The thick orange line shows the location of the sun over the integration

period and the thin orange line shows the terminator at the midpoint of the image integration. Regions of the image between the terminator and the new pole are on the dayside (ionospheric daytime), even if they map to a night side magnetospheric local time. For example, in Figure 1b, there are little to no emissions seen in the sunlit region on the midnight side of the pole within the polar collar. This region experiences a daytime ionospheric local time (it is sunlit), while simultaneously being connected to the night side magnetosphere.

2.3. Juno UVS' Views of the Poles

Using the magnetospheric local time projections of the data, we present observations of Jupiter's northern aurora (tilted over as it is toward ∼180° System III longitude) at approximately midnight (PJ8), dawn (PJ7), noon (PJ6), and dusk (PJ9) ionospheric local time (Figure 2). The ionospheric local times can best be tracked looking at the terminator lines shown in Figure 2. For PJ6, when the aurora (180° longitude) is oriented most closely to ionospheric noon, the majority of the auroral oval is illuminated by the sun, while for PJ8, when the aurora is oriented most closely to ionospheric midnight (subsolar longitude ∼0°), the majority of the oval is in darkness. While similar geometries to the ionospheric noon and dusk orientations in Figure 2 have been captured by HST many times in the past, only Juno could capture the midnight and dawn views shown in Figure 2. To compare images of Jupiter's aurora with distinctly different local time geometries, we must use images from multiple perijoves because the observation window for a given perijove is limited to a few hours. As Juno's orbit evolves over the course of the mission, the observation window for the northern polar region has been shrinking, decreasing coverage. However, the precession of the orbit is also positioning Juno at lower altitude over the north pole on each consecutive perijove, improving the spatial resolution of the maps over time. The situation is reversed in the south with viewing times increasing along with increasing spacecraft altitudes giving correspondingly lower spatial resolution maps. We present four south polar images in Figure 3 showing the local time variations in the south.

3. Results

3.1. The Polar Regions Redefined

When most of the auroral oval is sunlit, the color ratio maps of the northern aurora (PJ6, Figure 2) display a striking dichotomy between the "swirl region" and the "polar collar." The swirl region exhibits a high color ratio of ≥12, approximately encircled by the magenta line in the PJ6 images in Figure 2. The polar collar, outside of the swirl region but still within the main auroral oval, exhibits a low color ratio, ≤4 (cf. Bonfond et al., 2017). While most obvious in the ionospheric noon-dusk view of the northern aurora where the swirl region emissions are brightest (PJ6 and PJ9, Figure 2), this pattern is still evident at other ionospheric local times (see supplementary material). In this paper we consider the previously defined dark polar region and active region (see labels in PJ6 data, Figure 2; Grodent, 2015) to be part of a single region that we call the "polar collar," as we expect these two regions map to roughly similar radial distances in the magnetosphere and they exhibit the same color ratio emissions. The prime difference between the dark and active regions is a magnetospheric local time dependence, which we will discuss in the next section. The boundary between the swirl region and the polar collar is usually sharp and well defined in the color ratio maps, but is unremarkable in the brightness maps. This is especially noticeable on the dusk side where the polar collar emissions are similar in brightness to the dusk swirl-region emissions (PJ6 and PJ9, Figure 2).

3.2. Polar Collar

Focusing now on the brightness maps of Figure 2 and the extra images in the supplementary material, it is striking that the polar collar emission shows strong (order of magnitude) magnetic local time dependence at all ionospheric local times (all subsolar longitudes). The Juno UVS map from PJ6 looks much like earlier observations taken from HST showing little to no emission on the dawn side of the polar collar (Swithenbank-Harris et al., 2019) until mid-morning where the polar collar emissions increase and can become as bright as the main emission. These emissions remain enhanced until late evening, ∼21 hr magnetospheric local time, where they are observed to become much weaker. This local time variation gave rise to the dark and active region designations (Grodent et al., 2003). However, it could not be conclusively shown from HST observations alone if the polar collar always responds to magnetospheric local time drivers or if there is also a dependence on ionospheric local time. For the first time, the Juno UVS observations show that this polar collar emission structure is retained

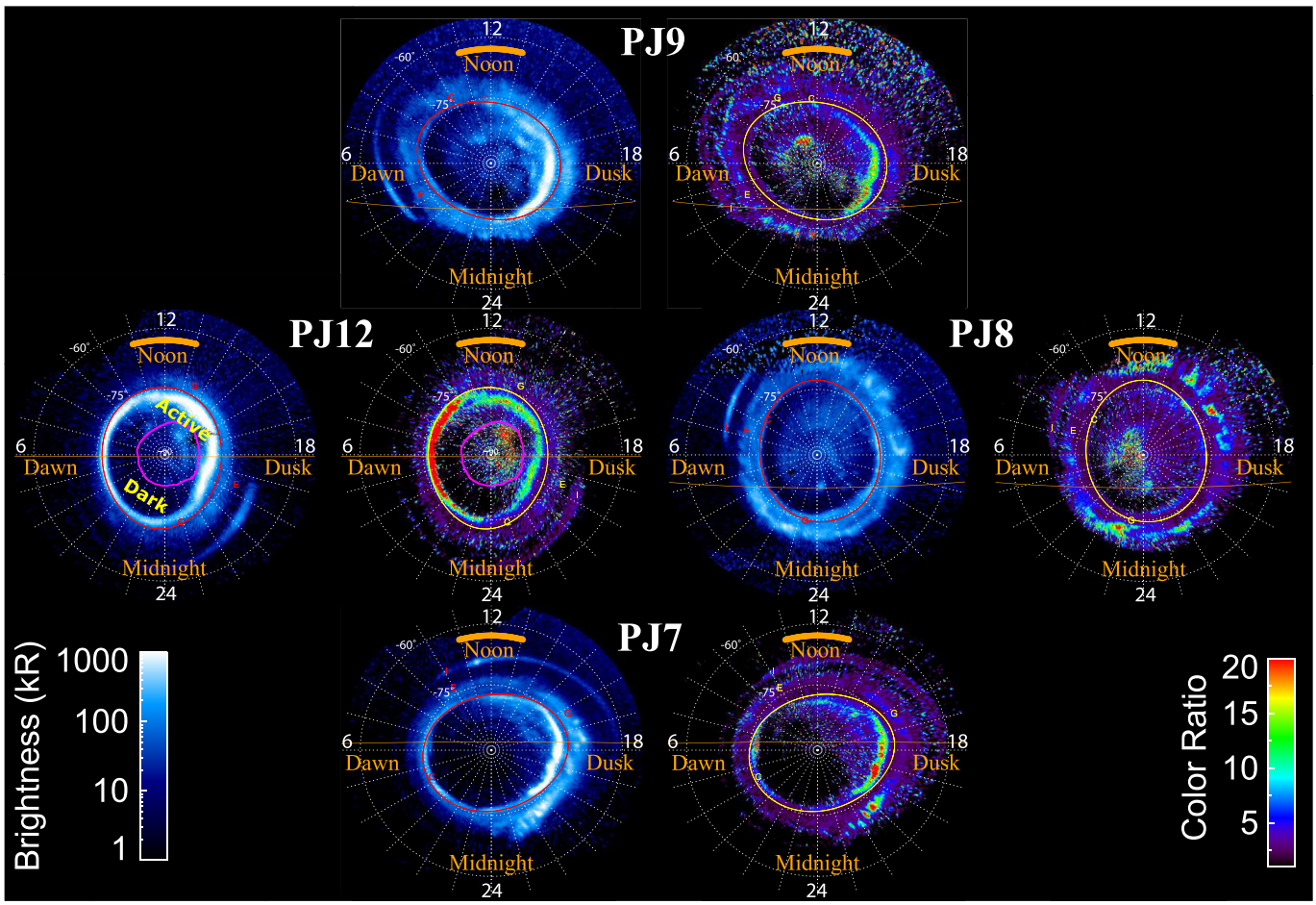

Figure 3. In these maps of the southern aurora, we have kept dawn on the left and dusk on the right, but have flipped noon and midnight relative to the plots of the northern aurora (Figure 2) with noon now pointed toward the top of the page. These maps are as would be seen from the spacecraft looking up at Jupiter's south pole. All the additional information (terminator, Callisto footprint path, local time, etc.) are the same as described in Figures 1 and 2. Times and spacecraft/Jupiter geometric details for all figures are listed in Table 1. The approximate demarcation between swirl region and polar collar is outlined in magenta in the PJ12 data at the left of the figure, and the dark and active regions making up the polar collar are labeled in the PJ12 brightness map.

throughout all auroral ionospheric local times, even when the entire polar collar is on the night side of Jupiter (i.e., PJ7 and PJ8 in Figure 2), strongly supporting a magnetospheric rather than ionospheric local time driver for the emissions within the polar collar (Cowley et al., 2003). Additionally, the bright dusk-side polar collar emissions often organize into what appear to be concentric arcs alternating between higher and lower brightness, though all at relatively low color ratio. This behavior has been discussed at length in the literature, sometimes referred to as transient "inner ovals" (Nichols, Clarke, Gerard, Grodent, & Hansen, 2009). The Juno UVS observations show this behavior is independent of System III longitude and ionospheric local time, and appears to be purely a magnetospheric dusk-side phenomenon, as shown in Figure 4 at two very different ionospheric local times. Short dusk arcs are also observed from noon to early evening on the dusk side of some southern auroral maps such as the one from PJ7 in Figure 3.

3.3. Swirl Region

Surprisingly, the brightness of the swirl region appears to be primarily correlated with subsolar longitude, unlike the polar collar emissions. Looking at Figure 5 and data in the Movie S1, the initial brightening of the swirl region occurs very close to the dawn terminator. The terminator shown in the figures is calculated at 400 km above the 1-bar level, about the altitude of the auroral emissions. The swirl region remains bright throughout the time it is sunlit and for several hours after sunset (Figure 2) when the emissions then fade to a low-level background state. This suggests that the swirl region's brightness is affected by the amount of sunlight incident on the upper

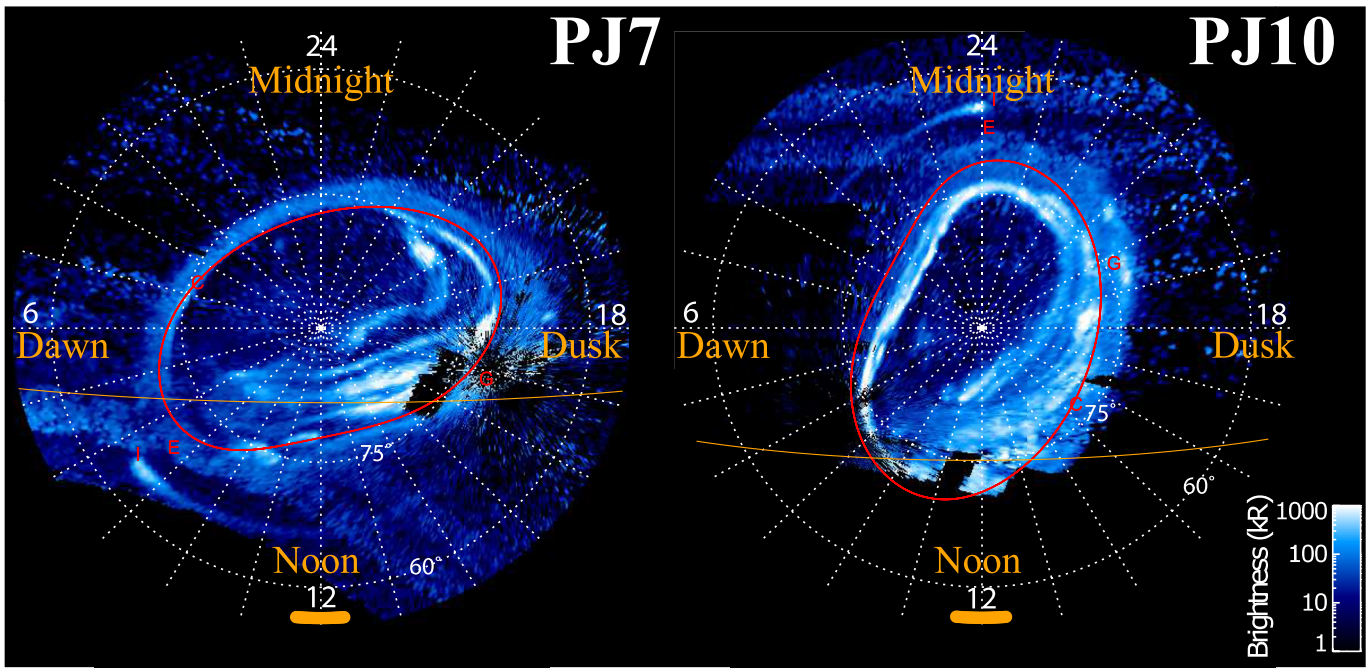

Figure 4. UV brightness maps from 31 spin (15.5 min) integrations of PJ7 and PJ10 observations. The dusk side concentric arcs within the polar collar are obvious in both, even though the System III longitudes and ionospheric local times are completely different.

atmosphere, perhaps through photoionization-induced conductivity. It does not appear to be under magnetospheric local time control, as evidenced by the fact that the entire swirl region is bright at the bottom of Figure 2, with swirl region emissions bright even when mapped on the magnetospheric night side. The opposite is true when the swirl region is completely in the dark (top of Figure 2), showing the entire swirl region is dark including the area mapping to midday magnetospheric time. Interestingly, even though the brightness of the swirl region emissions

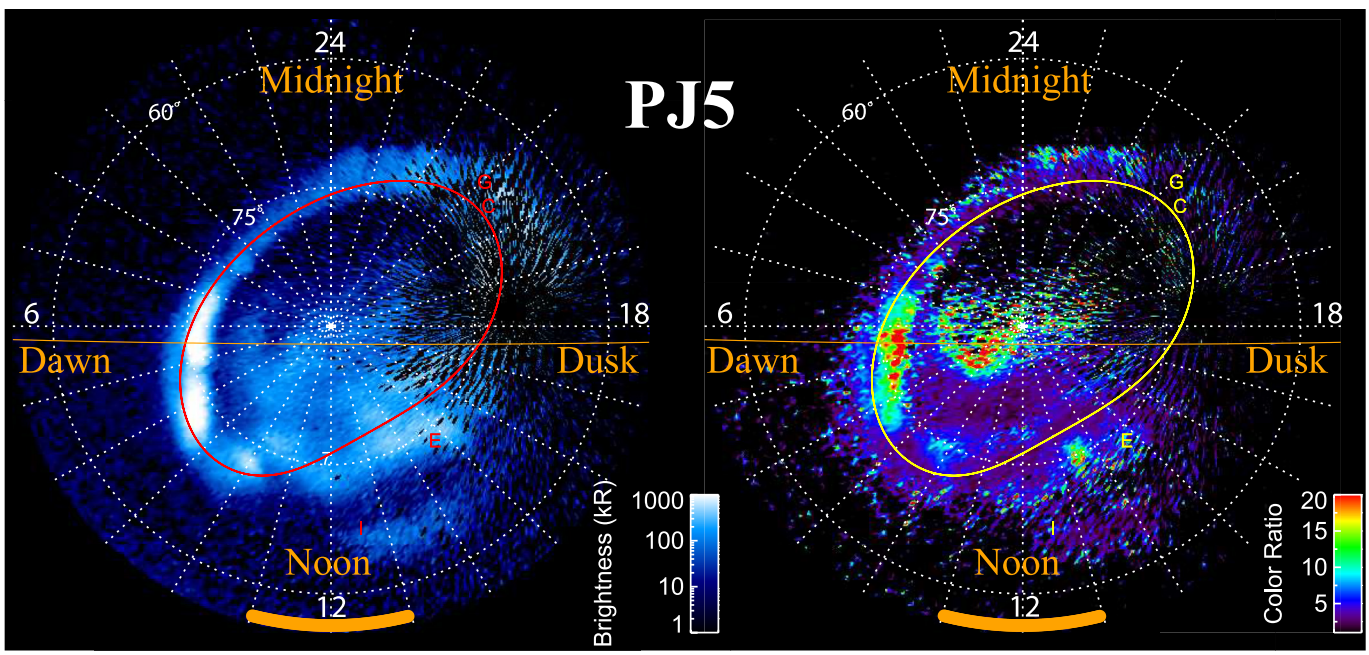

Figure 5. One of the best maps showing a portion of the swirl region brightening just as it crosses into sunlight. The majority of the swirl region is still in darkness exhibiting low emission brightness values.

Table 1
List of Midpoint Times, Spacecraft/Jupiter Range (Spacecraft to Jupiter Center Distances), and Sub-Solar System III Longitudes for Each Set of Auroral Images in Each Figure of the Main Text

Figure	Perijove	UTC time	Range (R_J)	Sub-solar longitude (deg)
1	5	27 March 2017 07:39:45	2.4	214
2	6	19 May 2017 03:59:13	3.6	135
	7	10 July 2017 23:55:58	3.5	42
	8	01 September 2017 20:14:06	3.0	322
	9	24 October 2017 16:59:30	1.7	259
3	7	11 July 2017 03:22:53	2.8	167
	8	01 September 2017 23:36:57	3.3	85
	9	24 October 2017 20:23:14	4.4	22
	12	01 April 2018 12:55:15	5.0	275
4	7	11 July 2017 00:48:07	2.3	74
	10	16 December 2017 16:45:43	2.4	305
5	5	27 March 2017 04:17:20	6.5	91
6	5	27 March 2017 07:39:45	2.4	214
7	3	11 December 2016 15:02:35	3.6	12
	13	24 May 2018 04:54:08	1.8	38

is significantly reduced between midnight and dawn, most of the faint emissions observed during this time period are still of high color ratio.

3.4. Southern Polar Emissions Compared to the North

Though the south polar emissions shown in Figure 3 are organized similarly to the north emissions described in the previous two sections, there are several differences worth noting. First is that the south polar emissions are generally much weaker than those in the north, as described by Grodent et al. (2018), and this is evident in the difference in emission strength and area between the northern and southern auroras shown in Figures 2 and 3. The center of the south polar oval is much closer to Jupiter's south-pole rotational axis, as compared to the north, reducing the strength of the modulation of solar flux over a Jovian rotation within the south-polar swirl region. Given the weaker fluxes in the south-polar region, it is more difficult to make clear statements on the turn-on and -off times for the southern swirl and polar collar emission, but in general our observations suggest similar timing as those viewed in the north.

4. Discussion

Given the low color ratio and magnetospheric local time control of the polar collar in comparison to the high color ratio and ionospheric local time control of the swirl region, it seems likely that the physical phenomena responsible for producing the emissions in the polar collar and swirl region are different. Is the color ratio boundary tracing a distinct transition in the outer magnetosphere? In an attempt to address this question we employ the Vogt magnetic flux mapping model (Vogt et al., 2011, 2015), updated to include the Jupiter JRM09 magnetic field model (Connerney et al., 2018). In Figure 6 we overlay the resultant local time and radial contours on top of brightness and color ratio maps from PJ5. We find that the red swirl region falls within the model contours suggesting it

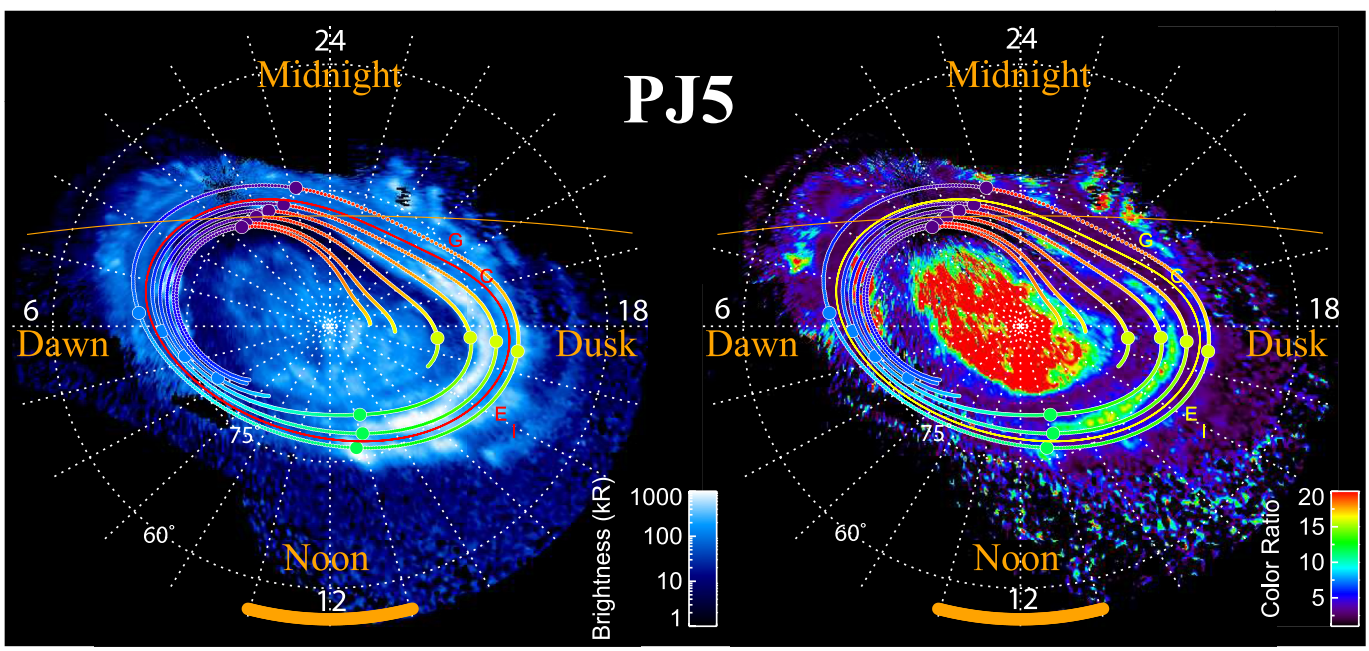

Figure 6. Observation of the north polar aurora taken during PJ5 similar in local time to that from PJ9 shown in Figure 2. Here we overplot Vogt et al.'s (2015) model contours corresponding to 15, 45, 75, 105, 135, and 150 R_J from outermost to innermost on the figure. Each contour is color coded in rainbow fashion to denote local time in the magnetosphere (purple = 0 hr, green = 12 hr, and red = 24 hr). The purple, blue, green and yellow dots on the contour indicate midnight, dawn, noon and dusk in the magnetosphere, respectively.

maps to beyond 150 R_J or would map beyond the magnetopause on the dayside in that model, which could be interpreted as mapping to a region of open flux. Whether this region is truly open flux or just highly twisted flux ropes extending to extreme distances down the magnetotail (Isbell et al., 1984; McComas and Bagenal, 2007; Zhang et al., 2021) cannot be discerned here. Possibly future magnetospheric models will be able to resolve this boundary and explain the different dynamics on either side leading to the clear auroral color ratio dichotomy.

Several possibilities exist for producing the higher color ratio emissions within the swirl region. The first is that for some reason the downward going magnetospheric electrons within this region are of higher energy than those observed over the polar collar. Higher energy electrons will travel deeper into Jupiter's atmosphere and excite the H_2 emissions at greater depth. These H_2 emissions would then exhibit a higher color ratio due to the absorption of CH_4 in the overlying atmosphere. While this is quite likely the simplest and most plausible reasoning, Juno to date has only rarely observed such a high-energy downward propagating electron population over the swirl region. To the contrary, Juno has primarily measured high energy, >1 MeV, electrons directed up from Jupiter's swirl region, but not a strong downward component (Clark et al., 2017; Mauk et al., 2020; Paranicas et al., 2018). It is possible that Juno has not yet gotten low enough over the northern swirl region to get below the acceleration region. If this is the case, Juno should be able to resolve the issue during the extended mission where the altitude of the northern auroral passes will continue to shrink. A second possibility is that the swirl region has a significantly different CH_4 vertical profile as compared to regions outside the swirl region. Several lines of evidence support the idea of a different CH_4 vertical structure associated with the auroral region (Clark et al., 2018; Moriconi et al., 2017; Sinclair et al., 2020). A sudden increase in the altitude of the CH_4 homopause relative to regions outside the swirl region would create a higher color ratio within the swirl region even for a uniform electron downward energy flux. However, as already stated, downward electrons have only rarely been found over the swirl region in amounts capable of reproducing the emissions observed in the UV (Ebert et al., 2019; Gérard et al., 2019). A third possibility is that sunlight would initiate/enhance photoionization of the upper atmosphere and in particular methane and other light hydrocarbons at the top of the neutral atmosphere. Ionization of the hydrocarbons would increase the ionospheric density at the base of the ionosphere, pushing the ionosphere deeper into Jupiter's upper atmosphere. This extension to greater depths coupled with aurorally driven Pedersen currents crossing the swirl region may be the cause of the high color ratio emissions if the collisions causing the H_2 emissions observed by UVS in the polar region are in fact coming from near the base of the ionosphere. However, this Pedersen current requires that ambient ionospheric ions carrying the current are accelerated to a few 10s of eV, in order to excite the H_2 emissions, which is difficult to do. Whatever the cause of the emissions, we observe that they brighten near sunrise and remain strong several hours of local time past sunset. It could be that the deeper ionospheric layer created during the day can exist well into the night due to a time lag in the recombination of the electrons and molecular hydrocarbon ions, or because some underlying current exists which would help support the extra ionization instigated by the sunlight during the daylight hours. Further evaluation of this and other possible explanations for the swirl region emissions goes beyond the scope of this observational paper. We leave it to future works to disentangle the exact mechanisms.

The description in Section 3.3 of the local time variability in the swirl region is true for most of the observations made by Juno UVS. However, there are a few observations where some unique emissions appear in the swirl region when it is positioned on the night side in the dark (midnight to dawn ionospheric local time). We show two such examples in Figure 7. Between the hours of ~2 and 6 magnetic local time, we have observed localized, high brightness, and lower color ratio (<8) emissions coming from discrete locations in the swirl region (examples circled in green in Figure 7). These observations sometimes show single spots of emission, as shown at the bottom of Figure 7, while other features have been seen to evolve over time to trace out swirls (top of Figure 7). Given their inconsistency (not seen in all instances, e.g., PJ7 and PJ8 in Figure 2) and their distinctive lower color ratio in the swirl region, which at most other times show emissions of high color ratio, we suspect these emissions are due to a distinct phenomenon occurring in the midnight to dawn sector of the magnetosphere and mapping to great radial distances, >150 R_J from comparisons with the Vogt JRM09 flux mapping results. The emission circled in PJ3 in Figure 7 has been characterized as a polar auroral bright spot by Haewsantati et al. (2021). As the Juno mission continues, we hope to observe such events while the spacecraft is connected to their magnetic field lines in order to sample the particles forming these emissions to help trace their origin and the reason for their different UV emission characteristics.

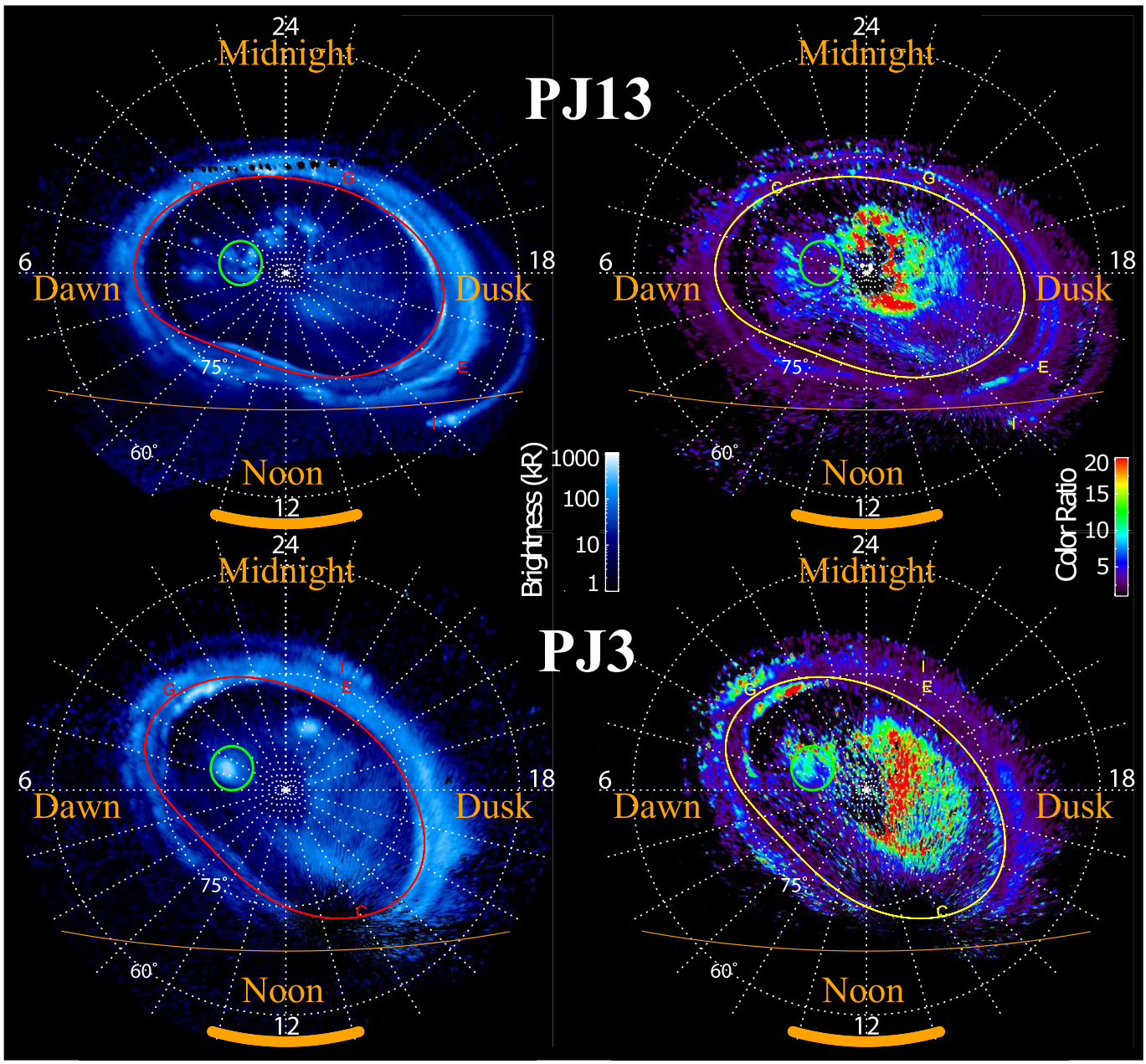

Figure 7. UV brightness and color ratio maps of the northern aurora from PJ3 (bottom) and PJ13 (top). The green circles enclose brightness anomalies, in what would generally be a low brightness period in the swirl region. The color ratio maps show that the emissions, though occurring in the swirl region, are of low to modest color ratio, quite different from the usual high color ratio emissions found there. While the green circles in a single pair of brightness and color ratio plots are in exactly the same place, there was no attempt to place them in the same position between PJ13 and PJ3. The fact that the circles in the two different observations are so close may be chance or may hint that both events have similar source regions in the outer magnetosphere, preferentially manifesting themselves at similar magnetospheric local time.

5. Conclusions

The imagery of Jupiter's northern and southern auroral zones captured from the unique vantage point of Juno UVS has produced an unbiased data set with which to study local time effects in Jupiter's magnetosphere. The global views of Jupiter's UV polar auroral emissions on the night side, at resolutions equal to or better than those captured on the dayside by HST, show the following key results:

1. The high color ratio of the polar swirl region makes it easily recognizable in UVS color ratio imagery in the middle of the northern auroral oval, and slightly offset in the southern auroral oval. The emissions in the polar

swirl region are generally bright from about 5-7 am until 20–22 hr ionospheric local time. The rest of the time, the emissions are an order of magnitude weaker or non-existent. It is interesting that the local time variation of these emissions are anti-correlated with the intense upward moving electron beams discussed by Bonfond et al. (2018) measured over the polar swirl region.

2. The polar collar, between the main emission and swirl region, shows magnetospheric local time control, with faint emissions observed from ~22 hr until mid-morning or noon, and bright emissions from noon until ~22 hr. Additionally, the region of bright emissions in the polar collar (previously called the active region) can exhibit arcs of emission concentric to or forking from the main emission (Nichols, Clarke, Gerard, Grodent, & Hansen, 2009). These concentric arcs may form at any System III longitude, but only on the dusk side of the polar collar (Figure 4). Similarly, we sometimes find concentric arcs of emission on the dusk side of the southern auroral polar collar like those in the north.
3. For brief periods, and only during some perijove passes, we observe intense, localized emissions from the polar swirl region between about 2 and 6 a.m. magnetic local time while the swirl region is positioned in darkness (ionospheric local time). Interestingly, these emissions can be of low color ratio. Given the low color ratio and local time of generation, it seems likely that they are produced by a separate phenomenon at large radial distances (>150 R_J) unrelated to the usual high-color-ratio emissions seen in the swirl regions when sunlit.
4. We observe that the intensity of the polar auroral emissions in the south are much reduced compared to those in the north in agreement with Grodent et al. (2018). This fact and the more poleward orientation of the southern aurora makes disentangling ionospheric and magnetospheric local time drivers difficult from southern hemisphere maps. However, the southern polar auroral emissions exhibit similar structures as the north with both a polar collar and swirl region. The local time control of these regions appears to agree with that in the north with the polar collar showing magnetospheric local time control and the swirl region exhibiting ionospheric local time control.

Data Availability Statement

The Juno data used in this study can be obtained from the Planetary Data System (PDS) at https://pds-atmospheres.nmsu.edu/data_and_services/atmospheres_data/JUNO/uvs.html. Specifically, the calibrated data (Trantham, 2014) was used and combined into the 101 spin integrated images for this study. The calibrated data is located https://pds-atmospheres.nmsu.edu/cgi-bin/getdir.pl?dir=DATA&volume=jnouvs_3001. All the 101 spin integrated images from Juno perijoves 1, 3–13 are included in the supporting materials to this article (Movie S1). The underlying data for the compiled images shown in the figures and supporting materials are archived (T.K. Greathouse, 2021) in idl save and FITS file formats.

Acknowledgments
This work was funded by NASA's New Frontiers Program for Juno via contract with the Southwest Research Institute. M.V. was supported by the Juno Participating Scientist program (grant number 80NSSC19K1263) and by NASA grant 80NSSC17K0777. B.B. is a Research Associate of the Fonds de la Recherche Scientifique - FNRS.

References

Acton, C. H. (1996). Ancillary data services of NASA's Navigation and Ancillary Information Facility. *Planetary and Space Science*, *44*(1), 65–70. https://doi.org/10.1016/0032-0633(95)00107-7

Allegrini, F., Gladstone, G. R., Hue, V., Clark, G., Szalay, J. R., Kurth, W. S., et al. (2020). First report of electron measurements during a Europa Footprint Tail Crossing by Juno. *Geophysical Research Letters*, *47*, e89732. https://doi.org/10.1029/2020gl089732

Allegrini, F., Mauk, G., Clark, G., Gladstone, G. R., Hue, V. R., Kurth, W. S., et al. (2020b). Energy flux and characteristic energy of electrons over Jupiter's Main Auroral Emission. *Journal of Geophysical Research (Space Physics)*, *125*, e27693. https://doi.org/10.1029/2019ja027693

Bagenal, F., Adriani, A., Allegrini, F., Bolton, S. J., Bonfond, B., Bunce, E. J., et al. (2017). Magnetospheric science objectives of the Juno Mission. *Space Science Reviews*, *213*, 219–287. https://doi.org/10.1007/s11214-014-0036-8

Bolton, S. J., Lunine, J., Stevenson, D., Connerney, J. E. P., Levin, S., Owen, T. C., et al. (2017). The Juno Mission. *Space Science Reviews*, *213*(1), 5–37. https://doi.org/10.1007/s11214-017-0429-6

Bonfond, B., Gladstone, G. R., Grodent, D., Gérard, J. C., Greathouse, T. K., Hue, V., et al. (2018). Bar code events in the Juno-UVS Data: Signature ~10 MeV electron microbursts at Jupiter. *Geophysical Research Letters*, *45*, 12108–12. https://doi.org/10.1029/2018gl080490

Bonfond, B., Gladstone, G. R., Grodent, D., Greathouse, T. K., Versteeg, M. H., Hue, V., et al. (2017). Morphology of the UV aurorae Jupiter during Juno's first perijove observations. *Geophysical Research Letters*, *44*(10), 4463–4471. https://doi.org/10.1002/2017GL073114

Bonfond, B., Grodent, D., Badman, S. V., Gérard, J. C., & Radioti, A. (2016). Dynamics of the flares in the active polar region of Jupiter. *Geophysical Research Letters*, *43*(2311), 963–970. https://doi.org/10.1002/2016GL071757

Bonfond, B., Vogt, M. F., Gérard, J. C., Grodent, D., Radioti, A., & Coumans, V. (2011). Quasi-periodic polar flares at Jupiter: A signature of pulsed dayside reconnections? *Geophysical Research Letters*, *38*(2). https://doi.org/10.1029/2010gl045981

Clark, G., Mauk, B. H., Paranicas, C., Haggerty, D., Kollmann, P., Rymer, A., et al. (2017). Observation and interpretation of energetic ion conics in Jupiter's polar magnetosphere. *Geophysical Research Letters*, *44*(10), 4419–4425. https://doi.org/10.1002/2016GL072325

Clark, G., Tao, C., Mauk, B. H., Nichols, J., Saur, J., Bunce, E. J., et al. (2018). Precipitating electron energy flux and characteristic energies in Jupiter's Main Auroral Region as Measured by Juno/JEDI. *Journal of Geophysical Research (Space Physics)*, *123*, 7554–7567. https://doi.org/10.1029/2018ja025639

Connerney, J. E. P., Kotsiaros, S., Oliversen, R. J., Espley, J. R., Joergensen, J. L., Joergensen, P. S., et al. (2018). A new model of jupiter's magnetic field from Juno's First Nine Orbits. *Geophysical Research Letters*, *45*, 2590–2596. https://doi.org/10.1002/2018gl077312

Cowley, S. W. H., & Bunce, E. J. (2001). Origin of the main auroral oval in Jupiter's coupled magnetosphere-ionosphere system. *Planetary and Space Science*, *49*, 1067–1088. https://doi.org/10.1016/s0032-0633(00)00167-7

Cowley, S. W. H., Bunce, E. J., Stallard, T. S., & Miller, S. (2003). Jupiter's polar ionospheric flows: Theoretical interpretation. *Geophysical Research Letters*, *30*, 24–21. https://doi.org/10.1029/2002gl016030

Ebert, R. W., Greathouse, T. K., Clark, G., Allegrini, F., Bagenal, F., Bolton, S. J., et al. (2019). Comparing Electron energetics and UV brightness in Jupiter's northern polar region during Juno Perijove 5. *Geophysical Research Letters*, *46*, 19–27. https://doi.org/10.1029/2018gl081129

Gérard, J.-C., Bonfond, B., Grodent, D., Radioti, A., Clarke, J. T., Gladstone, G. R., et al. (2014). Mapping the electron energy in Jupiter's aurora: Hubble spectral observations. *Journal of Geophysical Research: Space Physics*, *119*, 9072–9088.

Gérard, J.-C., Bonfond, B., Mauk, B. H., Gladstone, G. R., Yao, Z. H., Greathouse, T. K., et al. (2019). Contemporaneous observations of Jovian Energetic Auroral electrons and ultraviolet emissions by the Juno Spacecraft. *Journal of Geophysical Research: Space Physics*, *124*(11), 8298–8317. https://doi.org/10.1029/2019ja026862

Gladstone, G. R., Persyn, S. C., Eterno, J. S., Walther, B. C., Slater, D. C., Davis, M. W., et al. (2017). The Ultraviolet Spectrograph on NASA's Juno Mission. *Space Science Reviews*, *213*, 447–473. https://doi.org/10.1007/s11214-014-0040-z

Greathouse, T. K. (2021). *Local time dependence of Jupiter's polar Auroral emission observed by Juno UVS: Juno UVS Auroral images*. Mendeley Data. https://doi.org/10.17632/b36vz2ms3d.2

Greathouse, T. K., Gladstone, G. R., Davis, M. W., Slater, D. C., Versteeg, M. H., Persson, K. B., et al. (2013). *Performance results from in-flight commissioning of the Juno ultraviolet spectrograph (Juno-UVS)*.

Grodent, D. (2015). A brief review of ultraviolet Auroral emissions on giant planets. *Space Science Reviews*, *187*(1), 23–50. https://doi.org/10.1007/s11214-014-0052-8

Grodent, D., Bonfond, B., Yao, Z., Gérard, J.-C., Radioti, A., Dumont, M., et al. (2018). Jupiter's Aurora observed with HST during Juno Orbits 3 to 7. *Journal of Geophysical Research: Space Physics*, *123*, 3299–3319. https://doi.org/10.1002/2017ja025046

Grodent, D., Clarke, J. T., Waite, J. H., Cowley, S. W. H., GéRard, J.-C., & Kim, J. (2003). Jupiter's polar Auroral emissions. *Journal of Geophysical Research*, *108*. https://doi.org/10.1029/2003ja010017

Gustin, J., GéRard, J.-C., Grodent, D., Cowley, S. W. H., Clarke, J. T., & Grard, A. (2004). Energy-flux relationship in the FUV Jovian aurora deduced from HST-STIS spectral observations. *Journal of Geophysical Research (Space Physics)*, *109*. https://doi.org/10.1029/2003ja010365

Haewsantati, K., Bonfond, B., Wannawichian, S., Gladstone, G. R., Hue, V., Versteeg, M. H., et al. (2021). Morphology of Jupiter's Polar Auroral bright spot emissions via Juno-UVS observations. *Journal of Geophysical Research: Space Physics*, *126*(2), e2020JA028586. https://doi.org/10.1029/2020JA028586

Hill, T. W. (2001). The Jovian auroral oval. *Journal of Geophysical Research*, *106*, 8101–8107. https://doi.org/10.1029/2000ja000302

Hue, V., Gladstone, G. R., Greathouse, T. K., Kammer, J. A., Davis, M. W., Bonfond, B., et al. (2019). In-flight characterization and calibration of the Juno-Ultraviolet Spectrograph (Juno-UVS). *The Astronomical Journal*, *157*, 90. https://doi.org/10.3847/1538-3881/aafb36

Hue, V., Greathouse, T. K., Bonfond, B., Saur, J., Gladstone, G. R., Roth, L., et al. (2019). Juno-UVS observation of the IO footprint during solar Eclipse. *Journal of Geophysical Research: Space Physics*, *124*, 5184–5199. https://doi.org/10.1029/2018ja026431

Isbell, J., Dessler, A. J., & Waite, J. H., Jr. (1984). Magnetospheric energization by interaction between planetary spin and the solar wind. *Journal of Geophysical Research*, *89*, 10716. https://doi.org/10.1029/ja089ia12p10716

Mauk, B. H., Clark, G., Gladstone, G. R., Kotsiaros, S., Adriani, A., Allegrini, F., et al. (2020). Energetic particles and acceleration regions over Jupiter's Polar Cap and Main Aurora: A broad overview. *Journal of Geophysical Research (Space Physics)*, *125*, e27699. https://doi.org/10.1029/2019ja027699

McComas, D. J., & Bagenal, F. (2007). Jupiter: A fundamentally different magnetospheric interaction with the solar wind. *Geophysical Research Letters*, *34*, L20106. https://doi.org/10.1029/2007gl031078

Moriconi, M. L., Adriani, A., Dinelli, B. M., Fabiano, F., Altieri, F., Tosi, F., et al. (2017). Preliminary JIRAM results from Juno polar observations: 3. Evidence of diffuse methane presence in the Jupiter auroral regions. *Geophysical Research Letters*, *44*(10), 4641–4648. https://doi.org/10.1002/2017GL073592

Nichols, J. D., Badman, S. V., Bagenal, F., Bolton, S. J., Bonfond, B., Bunce, E. J., et al. (2017). Response of Jupiter's auroras to conditions in the interplanetary medium as measured by the Hubble Space Telescope and Juno. *Geophysical Research Letters*, *44*, 7643–7652. https://doi.org/10.1002/2017GL073029

Nichols, J. D., Bunce, E. J., Clarke, J. T., Cowley, S. W. H., Gérard, J.-C., Grodent, D., & Pryor, W. R. (2007). Response of Jupiter's UV auroras to interplanetary conditions as observed by the Hubble Space Telescope during the Cassini flyby campaign. *Journal of Geophysical Research (Space Physics)*, *112*, A02203. https://doi.org/10.1029/2006ja012005

Nichols, J. D., Clarke, J. T., Gérard, J. C., & Grodent, D. (2009). Observations of Jovian polar auroral filaments. *Geophysical Research Letters*, *36*(8). https://doi.org/10.1029/2009gl037578

Nichols, J. D., Clarke, J. T., Gérard, J. C., Grodent, D., & Hansen, K. C. (2009). Variation of different components of Jupiter's auroral emission. *Journal of Geophysical Research: Space Physics*, *114*(A6), a–n. https://doi.org/10.1029/2009ja014051

Paranicas, C., Mauk, B. H., Haggerty, D. K., Clark, G., Kollmann, P., Rymer, A. M., et al. (2018). Intervals of Intense Energetic Electron Beams Over Jupiter's Poles. *Journal of Geophysical Research (Space Physics)*, *123*, 1989. https://doi.org/10.1002/2017ja025106

Sinclair, J. A., Greathouse, T. K., Giles, R. S., Antuñano, A., Moses, J. I., Fouchet, T., et al. (2020). Spatial variations in the altitude of the CH_4 homopause at Jupiter's mid-to-high latitudes, as constrained from IRTF-TEXES Spectra. *The Planetary Science Journal*, *1*(3), 85. https://doi.org/10.3847/psj/abc887

Swithenbank-Harris, B. G., Nichols, J. D., & Bunce, E. J. (2019). Jupiter's Dark polar region as observed by the Hubble space telescope during the Juno Approach Phase. *Journal of Geophysical Research: Space Physics*, *124*, 9094.

Szalay, J. R., Allegrini, F., Bagenal, F., Bolton, S. J., Bonfond, B., Clark, G., et al. (2020). Alfvénic acceleration sustains Ganymede's footprint tail Aurora. *Geophysical Research Letters*, *47*, e86527. https://doi.org/10.1029/2019gl086527

Szalay, J. R., Bonfond, B., Allegrini, F., Bagenal, F., Bolton, S., Clark, G., et al. (2018). In situ observations connected to the io footprint tail Aurora. *Journal of Geophysical Research (Planets)*, *123*, 3061–3077. https://doi.org/10.1029/2018je005752

Trantham, B. (2014). *Juno J UVS reduced data record V1.0*. NASA Planetary Data System. https://doi.org/10.17189/1518951

Vogt, M. F., Bunce, E. J., Kivelson, M. G., Khurana, K. K., Walker, R. J., Radioti, A., et al. (2015). Magnetosphere-ionosphere mapping at Jupiter: Quantifying the effects of using different internal field models. *Journal of Geophysical Research: Space Physics*, *120*, 2584–2599. https://doi.org/10.1002/2014ja020729

Vogt, M. F., Kivelson, M. G., Khurana, K. K., Walker, R. J., Bonfond, B., Grodent, D., & Radioti, A. (2011). Improved mapping of Jupiter's auroral features to magnetospheric sources. *Journal of Geophysical Research: Space Physics*, *116*, A03220. https://doi.org/10.1029/2010ja016148

Waite, J. H., Gladstone, G. R., Lewis, W. S., Goldstein, R., McComas, D. J., Riley, P., et al. (2001). An auroral flare at Jupiter. *Nature*, *410*, 787–789. https://doi.org/10.1038/35071018

Yung, Y. L., Gladstone, G. R., Chang, K. M., Ajello, J. M., & Srivastava, S. K. (1982). H_2 fluorescence spectrum from 1200 to 1700 A by electron impact - Laboratory study and application to Jovian aurora. *The Astrophysical Journal Letters*, *254*, L65–L69. https://doi.org/10.1086/183757

Zhang, B., Delamere, P. A., Yao, Z., Bonfond, B., Lin, D., Sorathia, K. A., et al. (2021). How Jupiter's unusual magnetospheric topology structures its aurora. *Science Advances*, *7*(15), eabd1204. https://doi.org/10.1126/sciadv.abd1204